batteries

MDPI

Article

Free-Standing and Binder-Free Porous Carbon Cloth (C-Felt) Anodes for Lithium-Ion Full Batteries

Venroy Watson [1], Yaw D. Yeboah [1], Mark H. Weatherspoon [2] and Egwu Eric Kalu [1,*]

[1] Department of Chemical and Biomedical Engineering, FAMU-FSU College of Engineering, 2525 Pottsdamer St., Tallahassee, FL 32310, USA; venroy.watson@intel.com (V.W.); yyeboah@eng.famu.fsu.edu (Y.D.Y.)
[2] Department of Electrical and Computer Engineering, FAMU-FSU College of Engineering, 2525 Pottsdamer St., Tallahassee, FL 32310, USA; weathers@eng.famu.fsu.edu
* Correspondence: ekalu@eng.famu.fsu.edu; Tel.: +1850-410-6327

Abstract: A priority area for low-cost LIBs is the commercial production of electrodes with a high cycle life and efficiency in an environmentally benign fashion and a cost-effective manner. We demonstrate the use of undoped/untreated, flexible, stand-alone, mesh-like carbon cloth (C-felt) as a potential alternative anode to commonly used graphite composite anodes (GRAs) in LIBs. The performances of commercial GRAs (9 m^2/g) and C-felt (102 m^2/g) were compared as anodes vs. $LiFePO_4$ (14.5 m^2/g) cathodes in the full battery. Half-cell test results determined appropriate mass ratios of 2:1 for GRAs ($LiFePO_4$/GRA) and 1:1 for C-felt ($LiFePO_4$/C-felt). At a 0.3 C discharge rate, the 1:1 ratio yielded a specific discharge capacity of 104 mAh/g, in contrast to 87 mAh/g for the 2:1 ratio for a full cell in the 100th cycle, corresponding to a retention of 82% for the 1:1 $LiFePO_4$/C-felt full cell and 70% for the 2:1 $LiFePO_4$/GRA full cell from their first specific discharge capacities. By varying the ratio of C-felt anode to $LiFePO_4$ cathode in a full cell and expressing the specific capacity in the 100th cycle as a function of the fraction of C-felt present (at a fixed amount of $LiFePO_4$), a maximum specific capacity was achieved at a fraction of C-felt equal to 0.542 or (1:1.18) $LiFePO_4$/C-felt or 106 mAh/g. This corresponds closely to the experimentally determined value and supports (1:1) $LiFePO_4$/C-felt full cell as an optimum ratio that can outperform the (2:1) $LiFePO_4$/GRA full cell in our test conditions. Hence, we present C-felt anode as a potential cost-effective, lightweight anode material for low-cost LIBs.

Keywords: lithium-ion battery; full cell; carbon cloth anode; lithium-ion phosphate; binder-free; high capacity

Academic Editors: Marco Giorgetti and Wei Lv

Received: 2 January 2025
Revised: 14 February 2025
Accepted: 6 March 2025
Published: 14 March 2025

Citation: Watson, V.; Yeboah, Y.D.; Weatherspoon, M.H.; Kalu, E.E. Free-Standing and Binder-Free Porous Carbon Cloth (C-Felt) Anodes for Lithium-Ion Full Batteries. *Batteries* **2025**, *11*, 111. https://doi.org/10.3390/batteries11030111

1. Introduction

Since the first commercial application of a lithium-ion battery (LIB) by Sony in 1991, this battery has dominated a wide range of applications, which include motor vehicles, grid storage, and electronics [1–3]. The worldwide research interest in LIBs [1–4] is due to their longer cycle life and high efficiency in comparison to the competing secondary batteries [4–8]. An area of research interest targeting the advancement of LIBs is aimed at cost reduction and performance improvement of the electrodes. Currently, carbon composite anodes dominate the LIB industry, and these composites are usually expensive to fabricate [4,9,10].

The use of graphite or other composites in a full or half-cell of an LIB commonly requires the formation of a composite comprising a binder, active material (e.g., graphite), and other conductive additives deposited on a current collector [11–13]. Binder choices are mainly subject to their potential stability and capacity to withstand degradation, without a requirement for them to be conductive. The use of a binder without any electrochemical

contribution causes a dead weight in composites since it lowers the total specific capacity of the electrode. Furthermore, the use of composite electrode requiring a metal current collector also decreases the battery energy density and is seen as an additional cost [4]. Because of LIBs' wide applications, a current high-priority area is to obtain LIB electrodes that are cost-effective, have a high cycle life and efficiency, are easy to implement commercially, and are produced in an environmentally benign fashion [12].

A search of the literature yielded limited scholarly articles focusing on full-cell research. Those that do mainly use a graphite composite as the anode. Given the above issues of electrode composites, it is conceivable that a carbon composite anode such as graphite may be a limiting component of the overall performances of LIBs. A key question then to ask is, "Is there a potentially cheaper alternative to the composite graphite anode, exhibiting the same or a better performance than the graphite composite anode when used in a full cell?" As alternatives, Si, Ge, Mg, Pb, Al, Sn, Sb, Pt, Ag, In, or Zn, and some of their oxides are commonly applied as anodes [13–19]. Even though metal and metal oxide anodes have been heavily investigated, they are far from being commercialized. This is due to innate issues such as the pulverization arising from extreme volume change during lithiation/delithiation (up to 200% in some cases) [12]. As a result, carbonaceous materials continue to dominate as anodes in full cells' applications and we are still faced with the challenges of obtaining LIB anodes with cost-effectiveness, that meet environmental standards, and that have a high cycle life and efficiency, as mentioned earlier.

In regard to identifying potential carbon anode materials, we propose that carbon cloth (C-Felt), a commonly used material in fuel cells [20] as electrodes, can potentially be used as a replacement for graphite composite anodes in LIBs. This is especially true for some low-cost LIB applications. Carbon felt/cloth is characterized by a light weight, low cost, high strength, and flexibility [21]. Other characteristics include chemical resistance and good electronic conductivity due to the Sp^2 carbon bonds present within the carbon structure [22]. Already, researchers such as Liu et al. and Zhang et al. have used carbon cloth anodes as a template to deposit lithium-storing metals in order to obtain a higher capacity than that of a graphite composite [22,23]. However, in the quest to obtain higher metallic performing anodes, C-felt has not been given serious consideration as a viable carbon anode material in a full operational battery, though such an electrode can offer a more cost-effective approach than the graphite composite anode method [24–28]. Although the cost of graphite is lower than that of carbon felt [29], the use of N-methyl-2-pyrrolidone (NMP) as the solvent and polyvinylidene fluoride (PVDF) as the binder material in the processing of graphite anode electrodes significantly raises the overall cost of production of Li-ion batteries. Both *PVDF and NMP are used for lithium-ion electrode slurry preparation. NMP has a high cost and high toxicity and is recycled at a high capital cost.* Thus, the cost factor for graphite electrode preparation includes those costs associated with the NMP, solvent recovery, recycling and its associated equipment, and the equipment needed to avoid explosions and fires in the use of NMP solvents. The total cost escalates with scale. Environmentally, NMP is a carcinogen and is known for its toxicity. On this basis, although the mass of carbon cloth required for each Li-ion electrode battery may be more expensive than the mass of graphite used for the same electrode, the cost of preparing the graphite electrode is far greater than that of carbon cloth.

In this study, we examine and present for the first time the electrochemical performance of a full LIB cell consisting of a lithium-ion phosphate cathode and C-felt anode and show that carbon felt is a potential effective, binder-free carbon anode for LIB full-cell applications. Our results also show that opportunities exist to explore the optimization of other parameters to achieve a high-performing Li-ion full-cell battery at a lower cost and in

environmentally benign conditions, which is superior to the use of a graphite electrode and the associated steps involved in the classical preparation of a graphite electrode.

2. Materials and Methods

2.1. Raw Materials and Electrode Fabrication

Ready-to-use graphite powder (Formula BT SLC 1520T) was purchased from Superior Graphite (Chicago, IL, USA). Woven, flexible, lightweight AvCarb 1071 HCB carbon cloth (C-Felt) was purchased from Fuel Cell Earth LLC (Waltham, MA, USA). The round density of the carbon cloth as provided by the manufacturer was 1.76 g/cm^3 while the thickness at 1 PSI was 356 µm. Conductive carbon was purchased from Imerys Graphite and Carbon (Willebroek, Belgium). Powdered, carbon-coated lithium-ion phosphate (C-LiFePO$_4$) and a graphite anode on a copper current collector were purchased from China Activation Lithium Battery Company Limited (CALB). Polyvinylidene fluoride (PVDF/KYNAR) was obtained from Arkema Incorporation (Radnor, PA, USA). We sourced 1.0 molar lithium hexafluorophosphate (LiF$_6$P) dissolved in ethyl carbonate and dimethyl carbonate from BASF Corporation (Florham Park, NJ, USA). In addition, a glass fiber separator was purchased from EL-CELL Corporation (Hamburg, Germany). All materials utilized in this experiment were of research grade and did not require further refinement.

We combined 19 g NMP (19 mL) with 1 g of PVDF overnight at 85 °C to dissolve the PVDF binder. This mixture corresponds to a 5 wt.% concentration of PVDF in solution. In order to obtain a composite containing 10 wt.% binder, 10 wt.% conductive carbon, and 80 wt.% graphite composites, known amounts of each of the components were mixed using a mortar and pestle for three hours to obtain a consistent slurry. The conventional Dr. Blade method was followed to obtain electrodes. Electrodes were cut using a 1.27 cm^2-diameter MTI Corporation disc cutter and placed under a vacuum in an oven at 120 °C for 12 h. Active material loading comprised 10 mg graphite composite per 1.27 cm^2 disc.

By following similar procedures, lithium-ion phosphate composite cathodes were also prepared. In order to achieve a composite containing 5% binder + 95% C-LiFePO$_4$, 4.75 g of C-LiFePO$_4$ and 5.5 g of PVDF solution were mixed using a mortar and pestle for three hours to obtain a consistent slurry. The slurry was pressed on an aluminum current collector using an MTI Corporation flat film machine and then dried at 85 °C for 12 h following the Dr. Blade method. Electrodes were pressed and cut using a 1.27 cm^{2-}diameter MTI disc cutter with active mass loading of 10, 15, and 20 mg per 1.27 cm^2 disc. The discs were placed under a vacuum in an oven at 120 °C for 12 h before storage in an argon-filled glovebox.

To compare the performance of the C-LiFePO$_4$ cathode (LiFePO$_4$) vs. the Li anode half-cell, two full-cell anodes were obtained. In the first instance, graphite anodes on a Cu current collector typically used conventionally in lithium full cells were purchased from CALB (Changzhou, China). Disc anodes of 1.27 cm^2 diameter with an active mass loading of 10 mg per 1.27 cm^2 were punched out of this conventional graphite anode. Second, a flexible, lightweight, binder-free carbon cloth anode for comparative use in another full cell was purchased from Fuel Cell Earth LLC (Danbury, CT, USA). Since the carbon cloths (C-Felt) were premade and ready to be used, they were cut into discs of 1.27 cm^2 diameter with an active mass loading of 10 mg to 15 mg. Graphite and C-felt anodes were dried under a vacuum in an oven at 120 °C for 12 h and then stored in an argon-filled glovebox for cell assembly.

2.2. Material Characterization

Following the fabrication and preparation of electrodes, morphological characterization of the electrodes was conducted. A Transmission Electron Microscope (JEM-ARM200cF, JEOL Ltd., Tokyo, Japan) was used to determine the morphology, crystallinity, and ele-

mental mapping of the carbon-coated $LiFePO_4$ powder from CALB. Furthermore, the morphology of the electrodes' surfaces was obtained using a ZEISS 1540 scanning electron microscope (SEM) (Zeiss, Oberkochen, Germany). The phase or structural characterization of the C-felt and graphite anodes was determined using X-ray diffraction (XRD), and the diffraction patterns were mapped using a Siemens model D500 θ-2θ goniometer (Siemens, Munich, Germany).

2.3. Electrochemical Characterization

To observe the electrochemical performances of all electrodes, three sets of coin cells (type CR 2032) were fabricated in an argon-filled glovebox. The first set of coin cells consisted of half-cells with Li metal as the anode and a $LiFePO_4$ cathode. The second group or set was a conventional full cell comprising a composite graphite anode and $LiFePO_4$ cathode while the third set of coin cells possessed a C-felt anode and $LiFePO_4$ cathode. We used 1 molar lithium hexafluorophosphate (LiF_6P) in dimethyl carbonate (DMC) and ethyl carbonate (EC) as the electrolyte in all the cells. A glass fiber membrane separator with a diameter of 18 mm and thickness of 1.55 mm was used. The electrochemical performance between 0.0070 V and 2.70 V was measured during charging and discharging of the coin cells using a Neware battery testing analyzer with 5 V and 10 mA as the unit's maximum voltage and current, respectively. This system was connected to a Compaq computer. Gamry Instruments Reference 3000 Potentiostat/Galvanostat/ZRA was used for cyclic voltammetry (CV) and electrochemical impedance spectroscopy (EIS) analysis. CV analysis was performed at 0.5 mV/s between 0 V and 2.75 V. Moreover, EIS was performed from 10^6 Hz to 0.01 Hz at 100% state of charge (4 V). The electrochemical performances were all investigated at room temperature without external influences.

3. Results and Discussion

3.1. Morphological Characterization

Figure 1 shows the TEM morphology and elemental mapping of the $LiFePO_4$ cathode powder purchased from CALB. Figure 1a shows $LiFePO_4$ nanoparticles of various sizes in nm- to μm-length scale. The $LiFePO_4$ nanoparticles seem to be embedded in a network of carbon sheets, and hence, the manufacturer refers to the sample as "carbon-coated $LiFePO_4$". A higher-magnification TEM in Figure 1b shows the lattice of the $LiFePO_4$ crystal. Interestingly, the edges of the particle do not show a coating or carbon layer around the $LiFePO_4$ nanoparticles, thus confirming our previous observation of a carbon network engulfing the particles. As is commonly known, $LiFePO_4$ has poor electronic conductivity and manufacturers usually coat its surface with some form of conductive C. Figure 1c shows the diffraction image, which indicates that $LiFePO_4$ possesses a single-crystal structure regardless of the particle size. A brightfield image representing the $LiFePO_4$ sample shows the location of the metal nanoparticles (NPs) and C in the composite (Figure 1e). Elemental mapping was performed, as shown in Figure 1e,f, to identify the elemental compositions of the $LiFePO_4$ powder. C, Li, P, O, and Fe were located in the respective maps. The C map shows that the nanoparticle is not individually coated in C, since C was not mapped where the nanoparticle was located. This further supports the observation that the NPs are embedded in a network of C sheets.

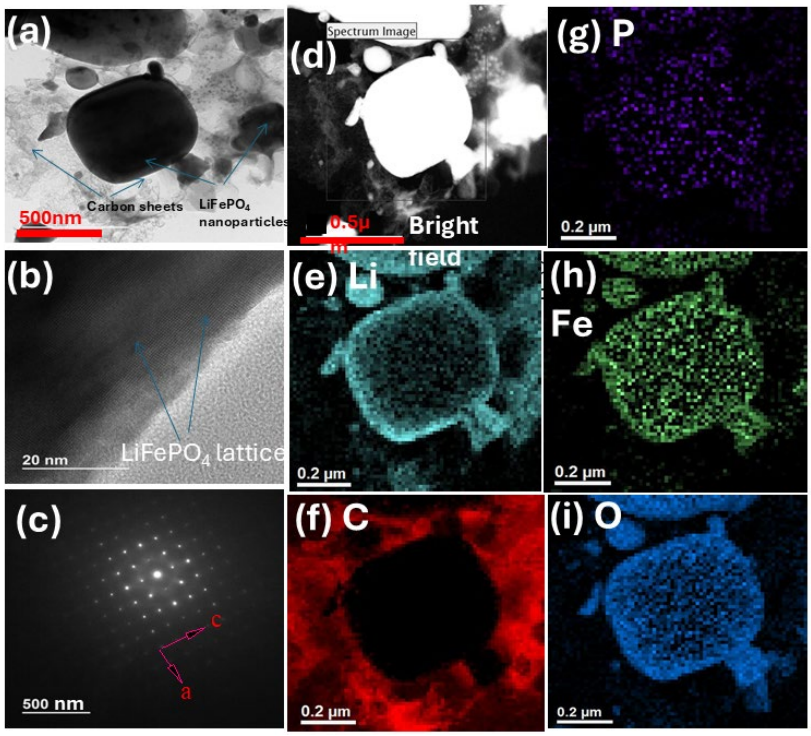

Figure 1. TEM morphology and elemental mapping of the $LiFePO_4$ cathode powder. (**a**) Carbon-coated $LiFePO_4$ nanoparticles. (**b**) Lattice of the $LiFePO_4$ crystal. (**c**) Diffraction image of the $LiFePO_4$ crystal. (**d**) Brightfield image of the $LiFePO_4$ sample. Elemental composition maps for (**e**) Li, (**f**) C, (**g**) P, (**h**) Fe, and (**i**) O.

Before the electrodes were used for half- and full-cell assembly, SEM characterization was also performed to better understand their morphologies, as can be seen in Figure 2. Figure 2a,b micrographs show that the graphite anode (GRA) is comprised of micron particle sizes. The C-felt anode morphologies at low and high magnifications can be seen in Figure 2c,d, respectively. At a low magnification, the SEM micrograph shows that C-felt has a network of intertwined C tubes, which is holding itself together without the use of a binder or any other reinforcement. The intertwined network adds porosity, flexibility, and mechanical stability to the free-standing C-felt anode material. At a high magnification, the C tubes appear to be of ~7 µm diameter with smooth and grooved surfaces. In addition, $LiFePO_4$'s cathode composite morphologies at low and high magnifications can be seen in Figure 2e,f, respectively. In Figure 2e, the micrograph shows that the composite has a uniform distribution of nanoparticles, while Figure 2f reveals that these NPs are closely bound together with sizes up to 300 nm.

Nitrogen adsorption/desorption isotherms for GRA, C-felt, and $LiFePO_4$ are shown in Figure 2h–i. Below 0.3 partial pressure, N_2 adsorption isotherms for the three samples show a straight line, suggesting a monolayer coverage, and from the slope of this region and the coverage, we were able to ascertain the BET surface area of each sample. BET analysis performed to determine the surface area of the electrodes shows that $LiFePO_4$ powder retrieved from the cathode had a BET surface area of 14.5 m^2/g, while CALB's graphite anode (GRA) scraped from the Cu current collector has a surface area of 9 m^2/g, and the C-felt surface area was found to be 102 m^2/g. The pore size distribution curves of the three samples are displayed in the inset of Figure 2h–i, where the sample inset curves show that all electrode materials had meso- to macropores with sizes ranging from approximately 25 nm to 300 nm. Above the 0.3 partial pressure, the isotherm deviates from the BET equation, suggesting a multilayer adsorption. All isotherms exhibit a hysteresis loop at

high pressure values. GRA exhibits a type V1 isotherm, while C-felt and $LiFePO_4$ exhibit a type 111 isotherm. All sample results were consistent and reproducible.

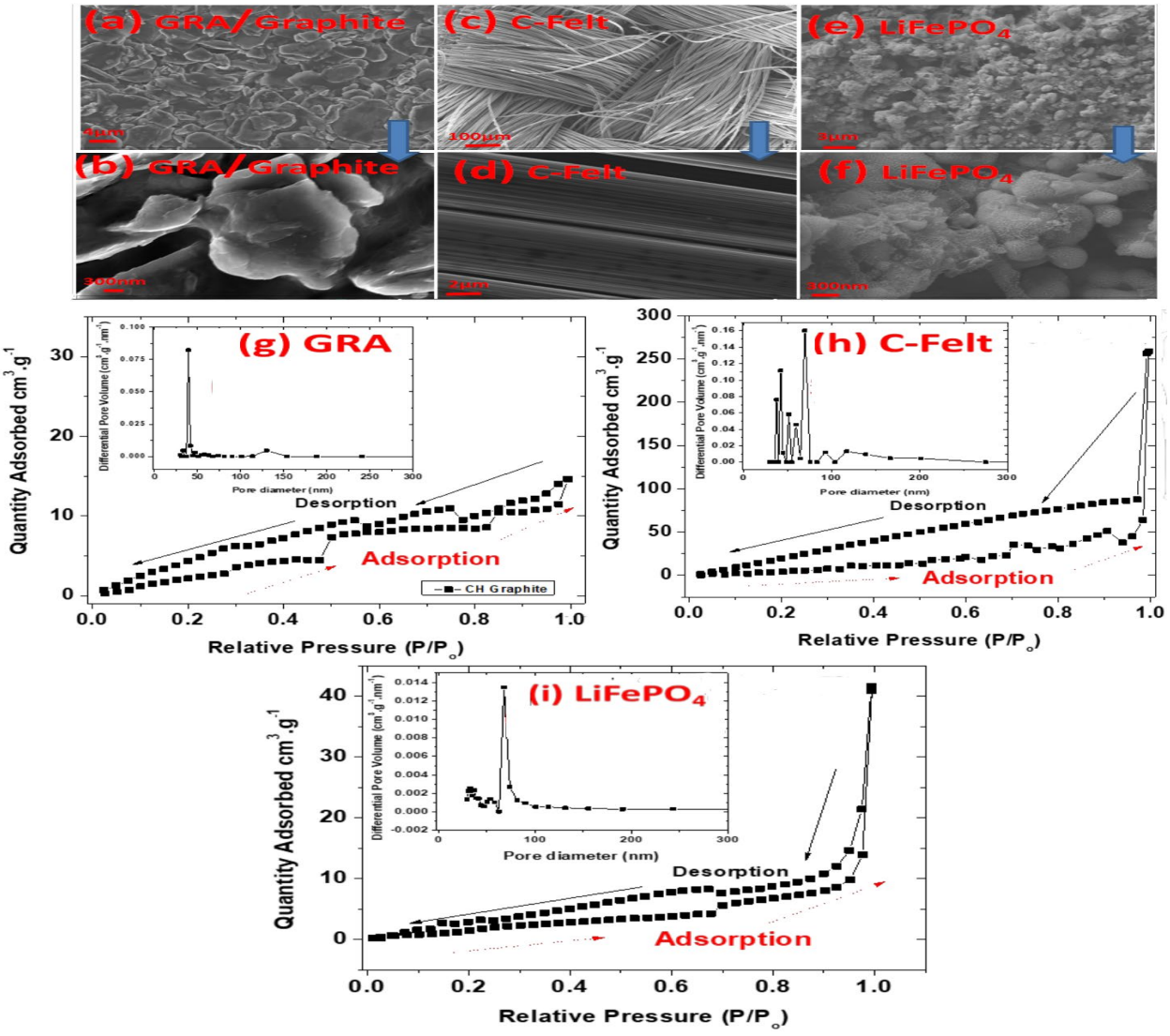

Figure 2. SEM images showing morphologies of (**a**) GRA at low magnification, (**b**) GRA at high magnification, (**c**) C-felt at low magnification, (**d**) C-felt at high magnification, (**e**) $LiFePO_4$ at low magnification, and (**f**) $LiFePO_4$ at high magnification. Nitrogen adsorption/desorption isotherms and BJH pore size distributions for (**g**) GRA, (**h**) C-felt, and (**i**) $LiFePO_4$.

XRD analysis was performed to determine the crystallinity of the anode materials, as shown in Figure 3. Figure 3a depicts the diffraction pattern of the C-felt material obtained commercially from Fuel Cell Earth. The dominant diffraction peak is located at 2 theta 26.5°, and this indicates a slightly graphitic nature of the C-felt. However, the broad peak tells us this anode is also amorphous. The graphitic characteristics of C-felt were expected since the MSDS and website state that the production of C-felt involves a long, high-temperature graphitization process. Graphite electrode powder retrieved from the current collector was tested by XRD, and we found the sharp diffraction peak associated with graphite located at 27° 2 theta.

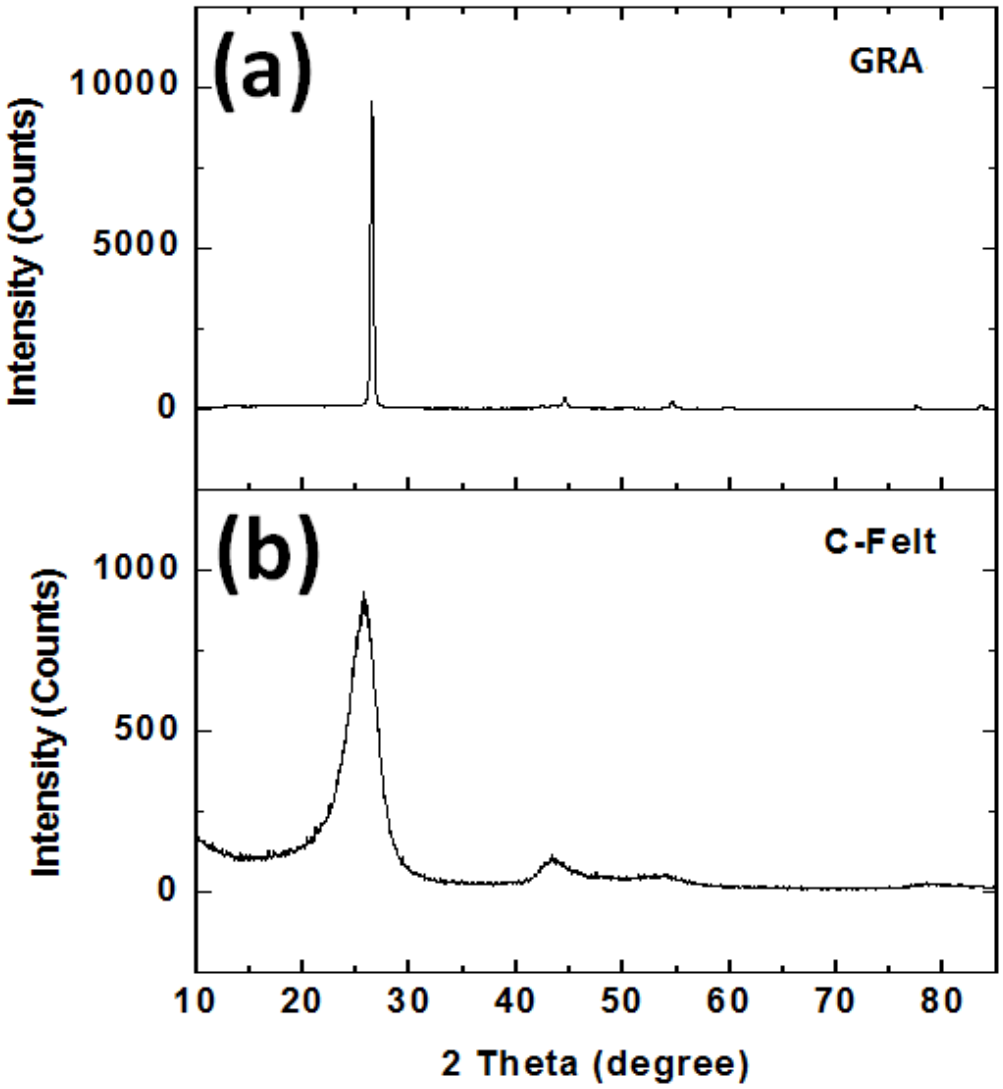

Figure 3. XRD patterns of (**a**) GRA and (**b**) C-felt.

3.2. Electrochemical Characterization of Half-Cells

To determine if the commercially obtained anodes and the in-house fabricated cathode were electrochemically active, cyclic voltammetry was performed at 0.5 mV/s, as shown in Figure 4, on half-cells with cathodes of graphite, C-felt, and $LiFePO_4$ vs. lithium metal anodes. Figure 4a,b show that those were tested between 0 V and 2.7 V. The GRA/Li half-cell in Figure 4a exhibits a lithiation peak close to 0 V with a decreasing voltage. In the opposite direction, the delithiation peak is centered at ~0.25 V. The C-felt/Li half-cell voltammogram curve undergoes lithiation, and the peak is highest as the voltage drops to 0 V (Figure 4b). This observation is like that in the GRA/Li half-cell. In the reverse direction, the delithiation peak of C-felt/Li is centered at 0.5 V. For the $LiFePO_4$/Li half-cell depicted in Figure 4c, lithiation and delithiation peaks are located between 2 V and 4 V as expected. Figure 4 demonstrates that all the electrodes assembled in half-cells are electrochemically active and reversible for the lithium electrochemical reaction, i.e., $yC + e^- + Li \rightleftharpoons LiC_y$

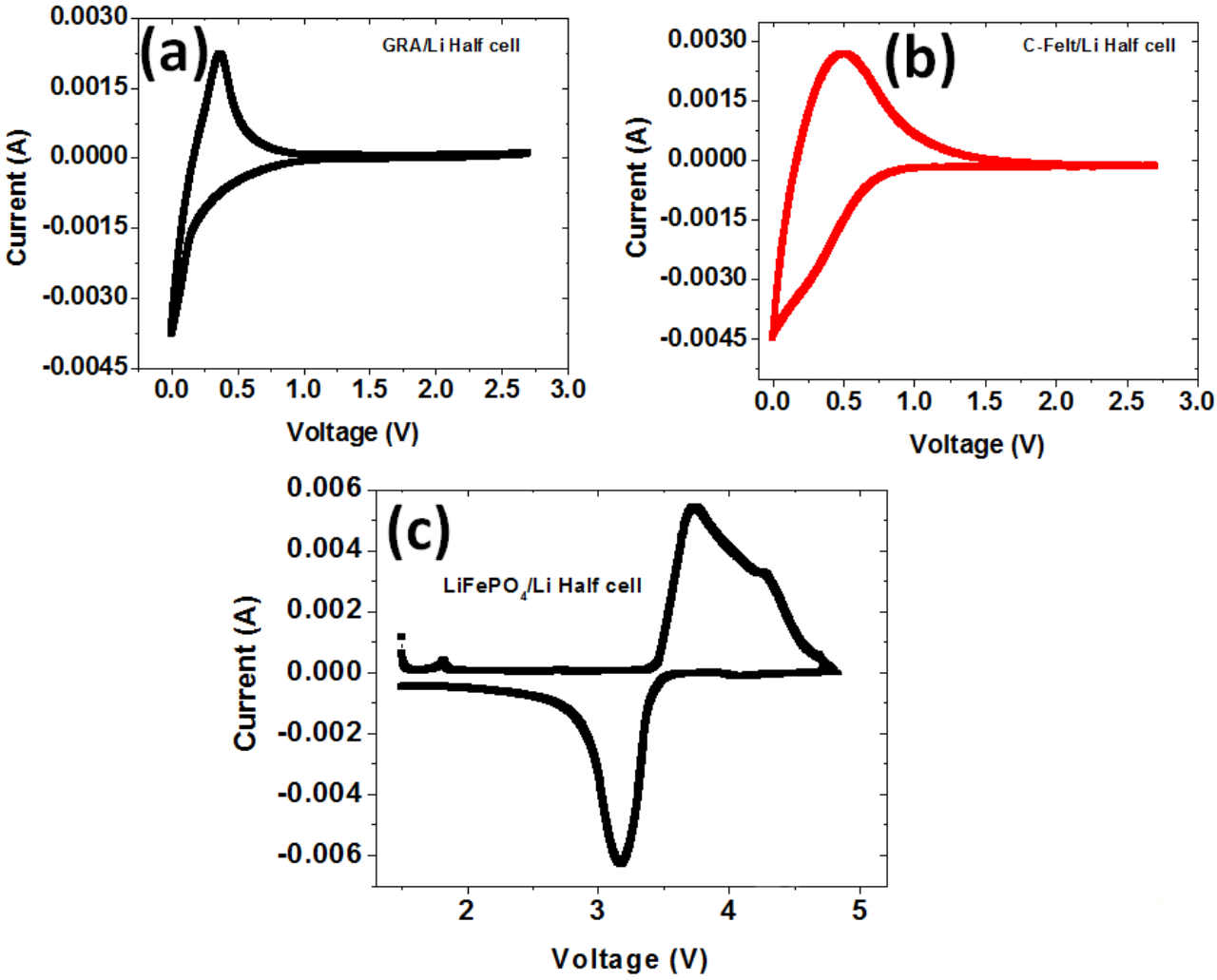

Figure 4. CV curves at 0.5 mV/s for half-cells using the Li anode with cathodes of (**a**) GRA, (**b**) C-felt, and (**c**) $LiFePO_4$.

To determine the specific capacity performance of the individual electrodes, half-cells were tested via charge/discharge analysis at a 40 mA/g current density, as plotted in Figure 5. The GRA/Li half-cell and C-felt/Li half-cell were first discharged from an as-prepared voltage to 0 V, and subsequent cycles were cycled between 1.2 V and 0 V. The $LiFePO_4$/Li half-cell was cycled between 2 V and 4 V. Specific capacities were determined with respect to the total weights of the electrodes including components such as active materials, binders, and conductive additives. Recall that in the case of the free-standing C-felt anode, no binder, conductive additives, or Cu current collector were used. While the active material of the cathode is $LiFePO_4$, the graphite and C-felt anode active material form the carbonaceous content of the electrodes. Our first-cycle charge/discharge analysis of the half-cells is shown in Figure 5a–c. Figure 5a shows GRA/Li half-cell charge and discharge first-cycle capacities of 265 mAh/g and 293 mAh/g, respectively. As expected, the discharge profile exhibited a relatively flat plateau below 0.3 V to 0 V, corresponding to the region of most capacity accumulation during lithiation. For the C-felt/Li half-cell, the first charge and discharge specific capacities are 129 mAh/g and 131 mAh/g, respectively. The discharge profile for a C-felt/Li half-cell has two regions of relative plateau. The upper plateau is located between 0.7 and 0.5 V. The second region of the discharge profile below 0.5 V begins to level off closer to 0 V, and this contributes most of the capacity accumulated. For both anodes, the first-cycle discharge is higher than the first-cycle charge, and this

is usually observed in anodic materials due to irreversible reaction pathways [4,30–32]. $LiFePO_4$/Li half-cell charge and discharge capacities were 139 mAh/g and 127 mAh/g, respectively. First-cycle charge exhibits a stable profile, leveling off at ~3.5 V, accumulating most of the capacity, and then rapidly increasing to 4 V. Similarly, in the discharge from 4 V, a constant profile was observed, located at ~3.3 V, and then a sharp decrease to 2 V. This stable plateau is characteristic of the $LiFePO_4$ performance and is of great importance in the discharging of the battery.

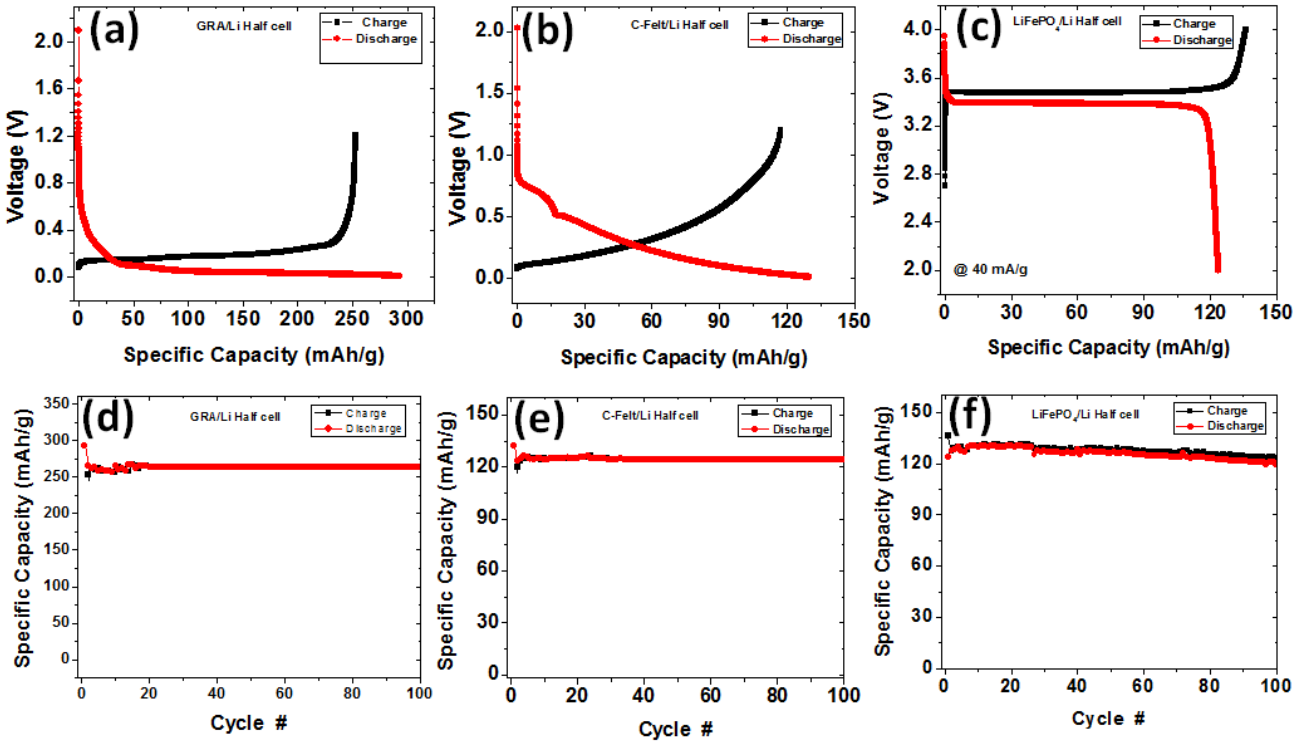

Figure 5. First-cycle charge/discharge profile of Li half-cell electrodes of (**a**) GRA, (**b**) C-felt, and (**c**) $LiFePO_4$. Charge/discharge performance at 40 mA/g for (**d**) GRA, (**e**) C-felt, and (**f**) $LiFePO_4$.

Following the first cycles of charge/discharge, all half-cells were cycled for up to 100 cycles to determine the stable reversible charge/discharge capacity of these electrodes at 40 mA/g (Figure 5d–f). All half-cells exhibited stable charge/discharge cycling from the 2nd to the 100th cycle with both the charge and discharge profiles overlapping, thus indicating the reversibility and high coulombic efficiency of the electrodes. For both the GRA/Li half-cell and C-felt/Li half-cell, the second-cycle discharge specific capacities were 265 mAh/g and 123 mAh/g, respectively. After 100 cycles, the discharge capacity exceeded 90% of the reversible second-cycle capacity, thus indicating that both anodes can cycle up to 100 cycles without significant capacity loss. For the $LiFePO_4$/Li half-cell, the specific discharge capacities were 127 mAh/g and 121 mAh/g after the 2nd and 100th cycles, respectively. This implies that the $LiFePO_4$/Li half-cell cathode can be cycled for up to 100 cycles while maintaining over 90% of the second-cycle capacity. To assemble full cells, the lithium source in the half-cells was changed from Li metal to $LiFePO_4$. Consequently, the differences in the reversible specific capacities of the carbonaceous (GRA and C-felt) anodes and the $LiFePO_4$ cathode demand a reasonable adjustment of the active masses of the electrodes to balance the discharge capacity [33–36] of the full cell. Additionally, capacity balancing can, as a safety measure, help prevent the risk of lithium plating and possible fire. Typically, that requires a slight oversizing of the capacity of the negative electrodes. The basic premise for capacity balancing is that the discharge capacity (in mAh)

is made equal for the negative and positive electrodes. Since the total capacity for each electrode is the product of the reversible specific capacity and used active mass, deductively, this means that the ratio of the specific capacity of the positive and negative electrodes is the inverse ratio of the respective masses, i.e.,

$$\frac{m_p}{m_n} = \frac{QC_n}{QC_p} \quad (1)$$

where m_p and m_n are the masses of the positive and negative electrodes, respectively, and QC_n and QC_p are the reversible specific charge capacities of the negative and positive electrodes, respectively. Hence, the charge balance requires the mass ratio between the anode electrode and $LiFePO_4$ cathode to be determined. To do this, the ratio of capacities from half-cells was used. Theoretically, the graphite and $LiFePO_4$ capacities are 372 mAh/g and 170 mAh/g, respectively. Hence, the theoretical capacity ratio of GRA/$LiFePO_4$ = 2.18. However, when using the half-cells' reversible second-cycle capacities, which are representative of the true test conditions in our experiments, we found a specific capacity balance for GRA/$LiFePO_4$ = 265/127 (mAh/g/mAh/g) = 2.08. Additionally, we found C-Felt/$LiFePO_4$ =124/127 (mAh/g/mAh/g) = ~1. Therefore, in order to assemble full cells using graphite anodes and C-felt anodes, vs. $LiFePO_4$ cathodes, from the capacity ratio calculated, the mass ratio of C-felt:$LiFePO_4$ used was 1:1, while the mass ratio of GRA:$LiFePO_4$ was 1:2.

3.3. Electrochemical Characterization of Full Cells

To properly test the use of the commercial anodes and the in-house fabricated cathode, full cells were assembled. However, such a full cell requires careful capacity balancing of the cathode (positive, P) and anode (negative, N) electrodes to help achieve the maximal specific energy outcome for the full cell as well as the minimal safety hazard (e.g., plating of Li on the negative electrode) [34]. The N/P ratio affects lithium plating during the charging process as well as the capacity and cyclability of the full cell. Thus, the effect of the negative to positive electrode ratio on the performance of a C-felt Li-ion full cell is of interest. Two full cells were first assembled with known mass ratios determined in Section 3.2: (a) (1:1) C-Felt:$LiFePO_4$ and (b) (1:2) GRA:$LiFePO_4$. To compare the performance of the C-felt electrode in a full cell, both full cells were tested at a current density of 40 mAh/g like the half-cells. The (2:1) $LiFePO_4$/GRA and (1:1) $LiFePO_4$/C-Felt full cells were cycled for up to 100 cycles and the results are shown in Figure 6. The (2:1) $LiFePO_4$/GRA first-cycle specific charge capacity was 135 mAh/g while its discharge specific capacity was 125 mAh/g. As can be seen in Figure 6a, both the charge and discharge curves were very close and overlapped, thus indicating a reversible capacity retention up to 100 cycles. After 100 cycles the specific charge and discharge capacities were lowered to 89 mAh/g and 87 mAh/g, respectively. The discharge capacity maintained 70% of the first-cycle capacity. For comparison, the (1:1) $LiFePO_4$/C-felt full cell charge/discharge profile is also shown Figure 6a. The specific capacities for the first-cycle charge and discharge are 139 mAh/g and 127 mAh/g, respectively. Like the (2:1) $LiFePO_4$/GRA full cell, the (1:1) $LiFePO_4$/C-felt full cell charge and discharge curves overlap, and after 100 cycles, the charge and discharge capacities decreased to 106 mAh/g and 104 mAh/g, respectively. The discharge specific capacity maintained 82% of the first-cycle capacity. As can clearly be seen, the (1:1) $LiFePO_4$/C-felt full-cell curve exhibited a higher capacity performance along with lower capacity loss than the (2:1) $LiFePO_4$/GRA full cell over the first 100 cycles shown. The (1:1) $LiFePO_4$/C-felt full cell has nearly a 20 mAh/g specific discharge capacity or 16% more discharge capacity than the (2:1) $LiFePO_4$/GRA full cell. This indicates that the C-felt anode when used in the above ratio can undergo long-term cycling with higher capacity

retention than the GRA. It is imperative to note that for both full cells, irrespective of the ratio used, the first charge and discharge capacities strongly correlate with the specific capacity determined for the half-cell of $LiFePO_4$. Clearly, the N/P ratio affects the specific discharge capacity of the full cell. Based on Equation (1), the mass ratios are inversely proportional to the capacity ratios of the electrodes.

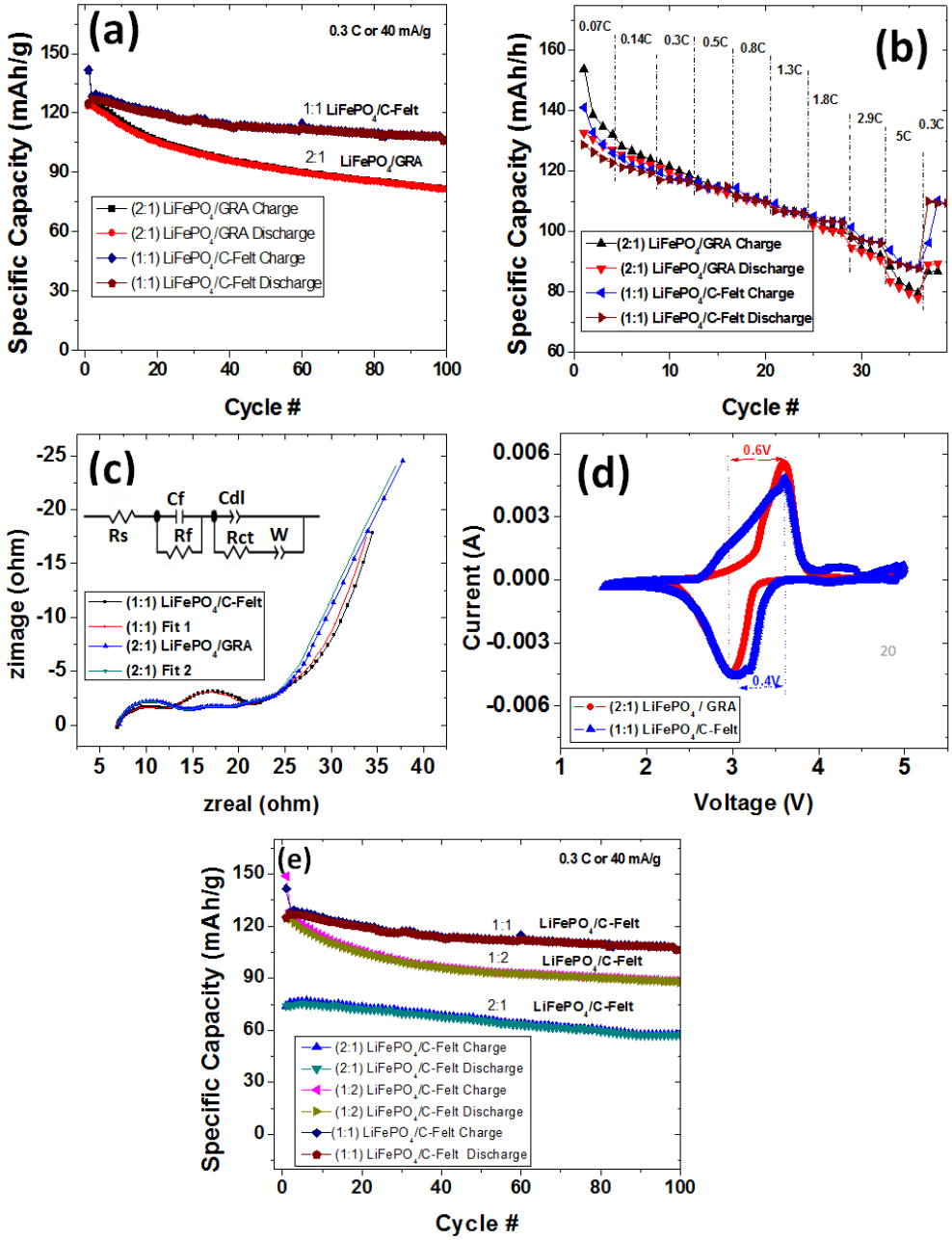

Figure 6. $LiFePO_4$/GRA and $LiFePO_4$/C-felt full-cell analysis. (**a**) Charge/discharge performance at 0.3 C (40 mA/g). (**b**) Rate performance from 0.07 C to 5 C. (**c**) Equivalent circuit model (ECM) and EIS analysis of full cells after 100 cycles. (**d**) CV analysis curves at 0.5 mV/s. (**e**) Charge/discharge performance of varying ratios of $LiFePO_4$ cathode to C-felt anodes at 0.3 C or a 40 mA/g rate.

The effect of the N/P ratio on the cyclability of the full cell is examined in Figure 6b.

In addition to cycling at 0.3 C (40 mAh/g), the (2:1) $LiFePO_4$/GRA full cell and the (1:1) $LiFePO_4$/C-felt full cell were charged and discharged at C rates ranging from 0.07 C to 5 C, as shown in Figure 6b. At a low C rate of 0.07 C, the $LiFePO_4$/GRA (2:1) full cell first-cycle charge and discharge capacities were 153 mAh/g and 131 mAh/g, respectively.

Similarly, the (1:1) $LiFePO_4$/C-felt at a low C rate exhibited first-cycle charge and discharged capacities of 127 mAh/g and 125 mAh/g, respectively. Interestingly, as the C rate increased to 0.14 C and 0.3 C, the (1:1) $LiFePO_4$/C-felt full-cell capacity approached the (2:1) $LiFePO_4$/GRA full-cell result. From 0.5 C to 1.3 C, both the (1:1) $LiFePO_4$/C-felt full-cell and the (2:1) $LiFePO_4$/GRA full-cell charge and discharge capacities overlapped. However, at 1.8 C to 5 C, the (1:1) $LiFePO_4$/C-felt full-cell specific capacities became higher than those of the (2:1) $LiFePO_4$/GRA full cell. At a 5 C rate, the (2:1) $LiFePO_4$/GRA full-cell first-cycle charge and discharge capacities decreased to 77 mAh/g and 75 mAh/g, respectively. Also, at a 5 C rate, the (1:1) $LiFePO_4$/C-felt full-cell first-cycle charge and discharge capacities decreased to 89 mAh/g and 87 mAh/g, respectively. This higher capacity performance by the (1:1) $LiFePO_4$/C-felt full cell may be ascribed to the higher surface area of the C-felt anode, which allows a larger surface area for taking part in electrochemical reactions (lithiation/delithiation) at high C rates. We arrive at this conclusion since the only difference between the two full cells is in the anodes used. Furthermore, the porous, mesh-like C-felt network along with the lack of binder may have rendered C-felt a better electronic and ionic transport medium than the composite graphite anode. As is commonly known, binders in composite anodes are electrochemically inactive, and inclusion of their weights in the total composite's weight also lowers the total specific capacity of the composite anodes.

Figure 6c shows the potentiostatic electrochemical impedance spectroscopy (EIS) following 100 cycles, which we used to determine the total impedance of the full cells. As is commonly known, EIS usually comprises solution resistance (Rs) intercepting the real *x*-axis, a semicircle associated with the charge transfer resistance (Rct), and a diffusion tail associated with the movements of ions in the electrodes [33]. In Figure 6c, both full cells exhibit an Rs of approximately 7.5 ohms in the high-frequency region. Following this, both full cells' EIS curves are characterized by two semicircles in the middle-frequency region. The combined semicircles corresponding to Rct are located at 20 ohms and 24 ohms for the (1:1) $LiFePO_4$/C-felt full cell and the (2:1) $LiFePO_4$/GRA full cell, respectively. The lower resistance could support the higher capacity exhibited by the $LiFePO_4$/C-felt full cell. In the low-frequency area, both batteries exhibit a sloping tail of approximately 45° associated with the diffusion of Li ion in the electrodes. Overall, the EIS results do not show much difference in the behavior of the two full cells.

The reversibility of the redox reaction occurring within these full cells was investigated via cyclic voltammetry at 0.5 mV/s (Figure 6d). It is commonly known that the ability of electrodes to be lithiated and delithiated (reversibility) can be assessed by the differences between the voltages of cathodic and anodic peaks. Here, the (1:1) $LiFePO_4$/C-felt and (2:1) $LiFePO_4$/GRA full cells exhibited oxidation and reduction peaks, and their respective voltage differences were found to be 0.4 V and 0.6 V. The lower voltage difference exhibited by the (1:1) $LiFePO_4$/C-felt full cell means the redox reaction occurs much faster in that cell's electrodes than in the (2:1) $LiFePO_4$/GRA full cell. This higher reversibility could be attributed to both the higher surface area for electrochemical reaction and lower resistance, which allow lithium ions to shuttle in and out of the C-felt anode, for example.

A further demonstration of the effect of N/P ratios on the capacity of the full cell is shown in Figure 6e where the charge/discharge profiles for the first 100 cycles of some $LiFePO_4$/C-felt full cells are compared. Here, (2:1) $LiFePO_4$/C-felt full cell and (1:2) $LiFePO_4$/C-felt full cell charge/discharge curves exhibit a similar initial capacity, and their overlap indicates a high coulombic efficiency. Briefly, with a focus on the discharge performance of the three full cells compared in Figure 6e, the first-cycle specific capacities were 127 mAh/g, 125 mAh/g, and 75 mAh/g for the (1:1) $LiFePO_4$/C-felt full cell, (1:2) $LiFePO_4$/C-felt full cell, and (2:1) $LiFePO_4$/C-Felt full cell, respectively. Regardless of the higher initial capacity exhibited by the (1:2) $LiFePO_4$/C-felt full cell, its capacity decreased

below that of the (1:1) $LiFePO_4$/C-felt full cell but remained higher than that of the (2:1) $LiFePO_4$/C-felt full cell, as shown by the discharge profiles. In the 100th cycle, the specific capacities of the respective full cells were 104 mAh/g, 89 mAh/g, and 59 mAh/g for the (1:1) $LiFePO_4$/C-felt full cell, (1:2) $LiFePO_4$/C-felt full cell, and (2:1) $LiFePO_4$/C-felt full cell, respectively. Also, the percentage capacity retention in the 100th cycle relative to the 2nd cycle was in order for the full cells: 81% for the (1:1) $LiFePO_4$/C-felt full cell, 71% for the (1:2) $LiFePO_4$/C-felt full cell, and 79% for the (2:1) $LiFePO_4$/C-felt full cell. Further, in Figure 7, a plot of the specific capacity data in the 100th cycle as a function of the fraction or relative amount of C-felt present in (at a fixed amount of $LiFePO_4$) the full cell $\left(\frac{C-Felt}{C-Felt+LiFePO_4}\right)$ suggests a functional relationship with a maximum specific capacity occurring at a fraction or relative amount of C-felt equal to 0.542, which is equivalent to a (1:1.18) $LiFePO_4$/C-felt ratio or 106 mAh/g. This is very close to the experimental value of (1:1) $LiFePO_4$/C-felt full cell observed and reported in Figure 6. With the above specific capacity results and the observed capacity retentions, we speculate that this ratio of C-felt provides the best storage accommodation for Li ions leaving or entering the cathode or electrolyte during the electrochemical redox process.

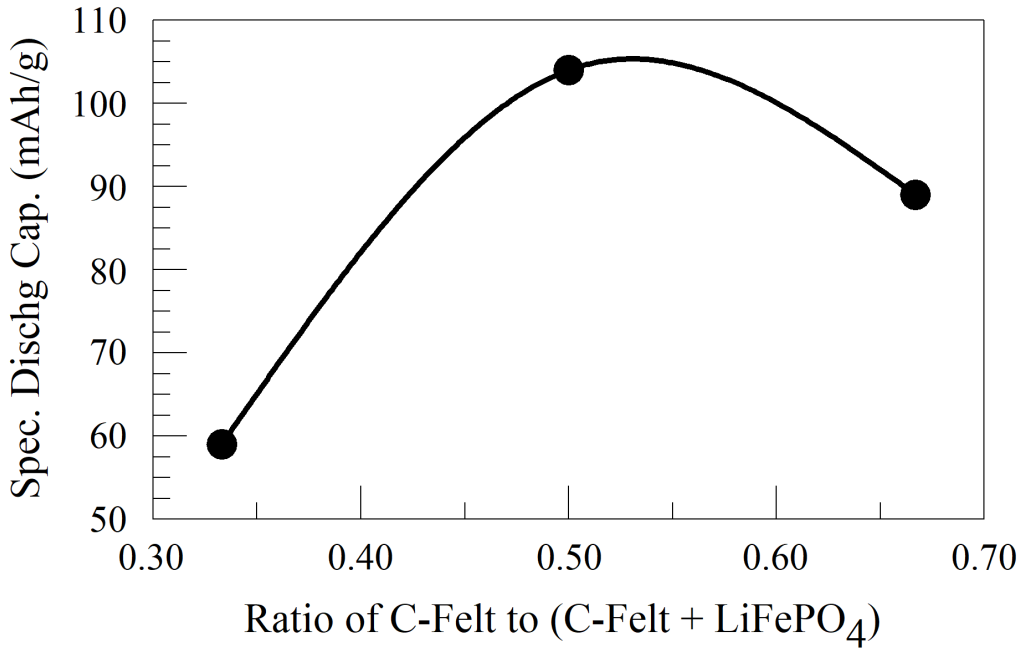

Figure 7. A plot of the specific capacity of a $LiFePO_4$/C-felt full cell in the 100th cycle as a function of the fraction or relative amount of C-felt.

4. Conclusions

We have successfully demonstrated that stand-alone, binder-free, and mesh-like C-felt anodes can be utilized in half and full battery assembly, as they perform well when compared with a conventional graphite composite anode. For full cells with the ratios of 1:2, 1:1, and 2:1 $LiFePO_4$ to C-felt when tested at 0.3 C, the specific discharge capacities after 100 cycles were 89 mAh/g, 104 mAh/g, and 59 mAh/g, respectively. On the other hand, a 2:1 ratio of $LiFePO_4$/GRA full cell when tested at the same rate yielded a specific discharge capacity of 87 mAh/g after 100 cycles. In addition, at 5 C, the (1:1) $LiFePO_4$/C-felt full cell outperformed the (2:1) $LiFePO_4$/GRA full cells. The result suggests a ratio close to (1:1) $LiFePO_4$/C-Felt for the optimal specific capacity performance of the $LiFePO_4$/C-felt full cell. The performance of the $LiFePO_4$/C-felt full cells could be ascribed to the high surface area and porous nature of the mesh-like network of carbon tubes in C-felt. The

above observations indicate that C-felt anodes can potentially be used in full cells as an alternative to a graphite composite anode, especially for low-cost Li-ion batteries. C-felt is a cost-effective material, and its use will limit the anode fabrication cost commonly associated with conventional high-cost wet chemistry synthesis methods used to fabricate graphite composite anodes after drying a slurry.

Author Contributions: Conceptualization, E.E.K. and V.W.; methodology, V.W.; software, V.W.; validation, E.E.K. and V.W.; formal analysis, V.W. and E.E.K.; investigation, V.W.; resources, E.E.K. and M.H.W.; data curation, V.W.; writing—original draft preparation, V.W.; writing—review and editing, E.E.K., M.H.W., and Y.D.Y.; visualization, V.W.; supervision, E.E.K. and Y.D.Y.; project administration, E.E.K.; funding acquisition, E.E.K. and M.H.W. All authors have read and agreed to the published version of the manuscript.

Funding: This research was funded by the ERC Program of the National Science Foundation under grant award number EEC-08212121.

Data Availability Statement: The original contributions presented in this study are included in the article, and further inquiries can be directed to the corresponding author.

Acknowledgments: The authors wish to acknowledge Dr. Eric Lochner (FSU Physics) and Bob Goddard (National High Magnetic Field Laboratory, Tallahassee) for their help with the XRD and SEM characterization, respectively. A portion of this work (TEM) was also performed by Xin Yan at the National High Magnetic Fields Laboratory, Tallahassee, Florida, which is supported by the National Science Foundation Cooperative (Agreement No. DMR-1644779) and the State of Florida.

Conflicts of Interest: The authors declare no conflicts of interest.

Abbreviations

The following abbreviations are used in this manuscript:

GRA Graphite Composite Anode

References

1. Padhi, A.K.; Nanjundaswamy, K.S.; Masquelier, C.; Okada, S.; Goodenough, J.B. Effect of Structure on the Fe^3/Fe^2 Redox Couple in Iron Phosphates. *J. Electrochem. Soc.* **1997**, *144*, 1609–1613. [CrossRef]
2. Padhi, A.K.; Nanjundaswamy, K.S.; Goodenough, J.B. Phospho-olivines as positive-electrode materials for rechargeable lithium batteries. *J. Electrochem. Soc.* **1997**, *144*, 1188–1194. [CrossRef]
3. Paul, R.; Etacheri, V.; Pol, V.G.; Hu, J.; Fisher, T.S. Highly porous three-dimensional carbon nanotube foam as a freestanding anode for a lithium-ion battery. *RSC Adv.* **2016**, *6*, 79734–79744. [CrossRef]
4. Yao, K.; Liang, R.; Zheng, J.P. Freestanding Flexible Si Nanoparticles–Multiwalled Carbon Nanotubes Composite Anodes for Li-Ion Batteries and Their Prelithiation by Stabilized Li Metal Powder. *J. Electrochem. Energy Convers. Storage* **2016**, *13*, 011004–011006. [CrossRef]
5. Armand, M.; Tarascon, J.M. Building better batteries. *Nature* **2008**, *451*, 652–657. [CrossRef]
6. Piao, Y.; Kim, H.S.; Sung, Y.-E.; Hyeon, T. Facile scalable synthesis of magnetite nanocrystals embedded in carbon matrix as superior anode materials for lithium-ion batteries. *Chem. Commun.* **2010**, *46*, 118–120. [CrossRef]
7. Xu, Y.; Zhu, Y.; Liu, Y.; Wang, C. Electrochemical Performance of Porous Carbon/Tin Composite Anodes for Sodium-Ion and Lithium-Ion Batteries. *Adv. Energy Mater.* **2013**, *3*, 128–133. [CrossRef]
8. Scrosati, B.; Hassoun, J.; Sun, Y.-K. Lithium-ion batteries. A look into the future. *Energy Environ. Sci.* **2011**, *4*, 3287–3295. [CrossRef]
9. Etacheri, V.; Wang, C.; O'Connell, M.J.; Chan, C.K.; Pol, V.G. Porous carbon sphere anodes for enhanced lithium-ion storage. *J. Mater. Chem. A* **2015**, *3*, 9861–9868. [CrossRef]
10. Campbell, B.; Ionescu, R.; Favors, Z.; Ozkan, C.S.; Ozkan, M. Bio-Derived, Binderless, Hierarchically Porous Carbon Anodes for Li-ion Batteries. *Sci. Rep.* **2015**, *5*, 14575. [CrossRef]
11. Yoshio, M.; Brodd, R.J.; Kozawa, A. *Lithium-ion Batteries*; Springer: Berlin/Heidelberg, Germany, 2009.
12. Sun, H.; Del Rio Castillo, E.A.; Monaco, S.; Capasso, A.; Ansaldo, A.; Prato, M.; Dinh, D.A.; Pellegrini, V.; Scrosati, B.; Manna, L.; et al. Binder-free graphene as an advanced anode for lithium batteries. *J. Mater. Chem. A* **2016**, *4*, 6886–6895. [CrossRef]

13. Pendashteh, A.; Tomey, R.; Vilatela, J.J. Nanotextile 100% Si Anodes for the Next Generation Energy-Dense Li-ion Batteries. *Adv. Energy Mater.* **2024**, *14*, 2304018. [CrossRef]
14. Omae, T.; Yamada, T.; Fujikake, D.; Kozawa, T.; Uchida, G. Development of nanostructured Ge/C anodes with a multistacking layer fabricated via Ar high-pressure sputtering for high-capacity Li^+ -ion batteries. *Appl. Phys. Express* **2024**, *17*, 026001. [CrossRef]
15. Kim, T.H.; Jeon, K.J.; Park, C.M. Black P@MO_x (M = Mg, Al, or Ti) composites as superior Li-ion battery anodes. *Chem. Eng. J.* **2021**, *424*, 130366. [CrossRef]
16. Arayamparambil, J.J.; Mann, M.; Liu, X.; Alfredsson, M.; Dronskowski, R.; Stievano, L.; Sougrat, M.T. Electrochemical Evaluation of Pb, Ag, and Zn Cyanamides/Carbodiimides. *ACS Omega* **2019**, *4*, 4339–4347. [CrossRef]
17. Lakshmia, D.; Nalinia, B.; Sivaraj, P.; Jayapandic, S. Electro analytical studies on indium incorporated SnSb alloy anode for Li-ion batteries. *J. Electroanalytical Chem.* **2017**, *801*, 459–465. [CrossRef]
18. Pan, W.; Yang, C.; Zhou, L.; Cai, X.; Wang, Y.; Tan, J.; Chang, J. Ag nanoparticle modified porous Si microspheres as high-performance anodes for Li-ion batteries. *Phys. Chem. Chem. Phys.* **2023**, *25*, 31754–31769. [CrossRef]
19. Park, C.; You, S.; Bae, J.-S.; Hur, J. Enhanced cycling reversibility and kinetics of indium oxide anode for Li-ion batteries using Zn doping and carbon composites. *J. Energy Storage* **2025**, *109*, 115238. [CrossRef]
20. Janicek, A.; Gao, N.; Fan, Y.; Liu, H. High Performance Activated Carbon/Carbon Cloth Cathodes for Microbial Fuel Cells. *Fuel Cells* **2015**, *15*, 855–861. [CrossRef]
21. Hu, L.B.; Wu, H.; Mantia, F.L.; Yang, Y.; Cui, Y. Thin, flexible secondary Li-ion paper batteries. *ACS Nano* **2010**, *4*, 5843–5848. [CrossRef]
22. Liu, B.; Zhang, J.; Wang, X.; Chen, G.; Chen, D.; Zhou, C.; Shen, G. Hierarchical Three-Dimensional $ZnCo_2O_4$ Nanowire Arrays/Carbon Cloth Anodes for a Novel Class of High-Performance Flexible Lithium-Ion Batteries. *Nano Lett.* **2012**, *12*, 3005–3011. [CrossRef] [PubMed]
23. Zhang, X.; Chen, S.; Yu, J.; Fang, D.; Zhang, S. A double-layered Ge/carbon cloth integrated anode for high performance lithium ion batteries. *RSC Adv.* **2016**, *6*, 63414–63417. [CrossRef]
24. Zhou, G.; Feng Li, F.; Cheng, H.-M. Progress in flexible lithium batteries and future prospects. *Energy Environ. Sci.* **2014**, *7*, 1307–1338. [CrossRef]
25. Pushnitsa, K.; Kosenko, A.; Chernyavsky, V.; Pavlovskii, A.A.; Novikov, P.; Popovich, A.A. Copper-Coated Graphite Felt as Current Collector for Li-Ion Batteries. *Coatings* **2022**, *12*, 1321. [CrossRef]
26. Fauteux, D.; Koksbang, R. Rechargeable Lithium Battery Anodes: Alternatives to Metallic Lithium. *J. Appl. Electrochem.* **1993**, *23*, 1–10. [CrossRef]
27. Chen, S.; Qiu, L.; Cheng, H.-M. Carbon-Based Fibers for Advanced Electrochemical Energy Storage Devices. *Chem. Rev.* **2020**, *120*, 2811–2878. [CrossRef]
28. Cheng, J.; Sun, H.; Chen, Y.; Kang, S.; Cui, L. Integrating N, P, Ni into 3D carbon felt anode for high-performance lithium metal batteries. *J. Alloys Comp.* **2024**, *977*, 173366. [CrossRef]
29. European Carbon and Graphite Association. Towards CO2 Neutrality Due to Carbon and Graphite 2018. Available online: https://ecga.net/ (accessed on 31 January 2025).
30. Forney, M.W.; DiLeo, R.A.; Raisanen, A.; Ganter, M.J.; Staub, J.W.; Rogers, R.E.; Ridgley, R.D.; Landi, B.J. High Performance Silicon Free-Standing Anodes Fabricated by Low-Pressure and Plasma-Enhanced Chemical Vapor Deposition onto Carbon Nanotube Electrodes. *J. Power Sources* **2013**, *228*, 270–280. [CrossRef]
31. Forney, M.W.; Ganter, M.J.; Staub, J.W.; Ridgley, R.D.; Landi, B.J. Prelithiation of Silicon-Carbon Nanotube Anodes for Lithium Ion Batteries by Stabilized Lithium Metal Powder (SLMP). *Nano Lett.* **2013**, *13*, 4158–4163. [CrossRef]
32. Guan, D.; Li, J.; Gao, X.; Yuan, C. Carbon nanotube-assisted growth of single-/multilayer SnS2 and SnO_2 nanoflakes for high performance lithium storage. *RSC Adv.* **2013**, *5*, 58514–58521. [CrossRef]
33. Kim, C.S.; Jeong, K.M.; Kim, K.; Yi, C.W. Effects of capacity ratios between anode and cathode on electrochemical properties for lithium polymer batteries. *Electrochim. Acta* **2015**, *155*, 431–436. [CrossRef]
34. Son, B.; Ryou, M.H.; Choi, J.; Kim, S.H.; Ko, J.M.; Lee, Y.M. Effect of cathode/anode area ratio on electrochemical performance of lithium-ion batteries. *J. Power Sources* **2013**, *243*, 641–647. [CrossRef]
35. Kasnatscheew, J.; Placke, T.; Streipert, B.; Rothermel, S.; Wagner, R.; Meister, R.; Laskovic, I.C. A tutorial into practical capacity and mass balancing of lithium-ion batteries. *J. Electrochem. Soc.* **2017**, *164*, A2479–A2486.
36. Geaney, H.; Bree, G.; Stokes, K.; McCarthy, K.; Kennedy, T.; Ryan, K.M. Highlighting the importance of Full-Cell testing for high performance anode materials comprising Li alloying nanowires. *J. Electrochem. Soc.* **2019**, *166*, A2784–A2790. [CrossRef]